

# Surface density of states and topological edge states in noncentrosymmetric superconductors

Keiji Yada,<sup>1</sup> Masatoshi Sato,<sup>2</sup> Yukio Tanaka,<sup>3</sup> and Takehito Yokoyama<sup>4</sup>

<sup>1</sup>Venture Business Laboratory, Nagoya University, Nagoya 464-8603, Japan

<sup>2</sup>Institute for Solid State Physics, University of Tokyo, Kashiwanoha 5-1-5, Kashiwa, Chiba 277-8581, Japan

<sup>3</sup>Department of Applied Physics, Nagoya University, Nagoya 464-8603, Japan

<sup>4</sup>Department of Physics, Tokyo Institute of Technology, Tokyo 152-8551, Japan

(Received 19 October 2010; published 11 February 2011)

We study an Andreev bound state (ABS) and the surface density of state (SDOS) of a noncentrosymmetric superconductor where spin-singlet  $d$ -wave pairing mixes with spin-triplet  $p$  (or  $f$ )-wave pairing by spin-orbit coupling. For  $d_{xy} + p$ -wave pairing, the ABS appears as a zero-energy state. The present ABS is a Majorana edge mode preserving the time-reversal symmetry. We calculate the topological invariant and discuss the relevance to a single Majorana edge mode. In the presence of the Majorana edge mode, the SDOS depends strongly on the direction of the Zeeman field.

DOI: 10.1103/PhysRevB.83.064505

PACS number(s): 74.45.+c, 74.50.+r, 74.20.Rp

## I. INTRODUCTION

Recently, physics of noncentrosymmetric (NCS) superconductors has been one of the important issues in condensed matter physics. Actually, several NCS superconductors have been discovered, such as CePt<sub>3</sub>Si,<sup>1</sup> Li<sub>2</sub>Pt<sub>3</sub>B,<sup>2</sup> and LaNiC<sub>2</sub>.<sup>3</sup> Also, the two-dimensional NCS superconductivity is expected at the interfaces of surfaces due to the strong potential gradient. An interesting example is the superconductivity at the LaAlO<sub>3</sub>/SrTiO<sub>3</sub> heterointerface.<sup>4</sup> In NCS superconductors, the spin-orbit coupling comes into play. One of the remarkable features is that due to the broken inversion symmetry, the superconducting pair potential becomes a mixture of spin-singlet even parity and spin-triplet odd parity.<sup>5</sup> Frigeri *et al.*<sup>6</sup> have shown that a  $p$  ( $p_x \pm ip_y$ )-wave pairing state has the highest  $T_c$  within the triplet channel in CePt<sub>3</sub>Si. Due to the mixture of singlet  $s$ -wave and triplet  $p$ -wave pairings, several novel properties such as the large upper critical field are expected.<sup>6,7</sup>

Several studies have addressed superconducting profiles for NCS superconductors.<sup>6-15</sup> In these works, pairing the symmetry of NCS superconductors has been mainly assumed to be a  $s + p$ -wave, where a spin-triplet  $p$  ( $p_x \pm ip_y$ )-wave and spin-singlet  $s$ -wave pair potential mix with each other as a bulk state. However, in a strongly correlated system, different types of pairing symmetries are possible. Microscopic calculations have shown that a spin-singlet  $d_{x^2-y^2}$ -wave pairing mixes with a spin-triplet  $f$ -wave pairing based on the Hubbard model near half filling.<sup>16</sup> The magnitude of spin-triplet  $f$ -wave pairing in this  $d_{x^2-y^2} + f$ -wave pairing is enhanced by a Rashba-type spin-orbit coupling originating from the broken inversion symmetry. Also, a possible pairing symmetry of superconductivity generated at the LaAlO<sub>3</sub>/SrTiO<sub>3</sub> heterointerface<sup>4</sup> has been studied based on a similar model.<sup>17</sup> In Ref. 17, it has been found that the gap function consists of a spin-singlet  $d_{xy}$ -wave component and spin-triplet  $p$ -wave one. The ratio of the  $d_{xy}$ -wave and the  $p_x$  ( $p_y$ )-wave component in this  $d_{xy} + p$ -wave model continuously changes with the carrier concentration.

Stimulated by these backgrounds, a study of Andreev bound states (ABSs) of  $d_{xy} + p$  or  $d_{x^2-y^2} + f$ -wave pairing has begun.<sup>18</sup> It has been known that the generation of ABSs

at the surface or interface is a remarkable feature specific to unconventional pairing<sup>19</sup> since an ABS directly manifests itself in the tunneling spectroscopy. Actually, for  $d_{xy}$ -wave pairing, a zero-energy ABS appears.<sup>20</sup> The presence of the ABS has been verified by tunneling experiments of high- $T_c$  cuprate<sup>20,21</sup> as a zero bias conductance peak.<sup>22</sup> For a chiral  $p$ -wave superconducting state realized in Sr<sub>2</sub>RuO<sub>4</sub>,<sup>23</sup> the ABS is generated as a chiral edge mode that has a dispersion proportional to the momentum parallel to the interface.<sup>24</sup> For  $s + p$ -wave NCS superconductors, when the magnitude of the  $p$ -wave pair potential is larger than that of the  $s$ -wave one, it has been shown that ABS is generated at its edge as helical edge modes similar to those in a quantum-spin Hall system.<sup>11-13,25</sup> Several new features of spin transport stemming from these helical edge modes also have been predicted.<sup>12-15</sup>

In Ref. 18, we have clarified the ABS and tunneling conductance  $\sigma_C$  in normal metal/NCS superconductor junctions for  $d_{xy} + p$ -wave and  $d_{x^2-y^2} + f$ -wave pairings. In both cases, new types of ABSs appear, in stark contrast to the  $s + p$ -wave case. In particular, for the  $d_{xy} + p$ -wave case, due to the existence of the Fermi surface splitting by spin-orbit coupling, a Majorana edge state appears with flat dispersion preserving the time-reversal symmetry. Reflecting the Majorana edge state,  $\sigma_C$  has a zero bias conductance peak in the presence of the spin orbit coupling.

Topological aspects of edge states have been attracting intensive interests in condensed matter physics. In particular, it was highlighted by the discovery of the quantum Hall system (QHS) showing the accurate quantization of the Hall conductance  $\sigma_H$ , which is related to the topological invariant.<sup>26,27</sup> It is known that the chiral edge state is generated at the edge of the sample. The concept of the QHS has been generalized to the time-reversal symmetric system, i.e., the quantum-spin Hall system (QSHS).<sup>25,28</sup> In QSHS, there exist helical edge modes, i.e., the time-reversal pair of right- and left-going one-dimensional modes. The edge modes are generated from the nontrivial topological nature of a bulk Hamiltonian and topologically protected. Furthermore, recently, pursuing the analogous nontrivial edge state including the Majorana edge mode in a superconducting system has become a hot issue.<sup>29-31</sup> Although there have been many studies of edge modes in topologically nontrivial superconducting systems,<sup>32-34</sup> the

relation between edge modes (ABSs) and the surface density of states has not been fully clarified.

In the present paper, we study the time-reversal invariant Majorana edge state in detail. In particular, we examine the local density of state at surface, i.e., the surface density of state (SDOS) for NCS superconductors with  $s + p$ ,  $d_{x^2-y^2} + f$ , and  $d_{xy} + p$ -wave pair potential, based on the lattice model Hamiltonian. It is known that the ABS appears as a zero-energy peak in SDOS, which is observable for tunneling spectroscopy in a high- $T_c$  cuprate.<sup>21,22</sup> It is quite important to clarify the SDOS and ABS for a new type of pair potentials that we will discuss in the present paper. For  $d_{xy} + p$ -wave pairing, we confirm that an unusual ABS appears as a zero-energy state due to the Fermi surface splitting by the spin-orbit coupling. The present ABS is a single Majorana edge mode preserving the time-reversal symmetry. In the presence of the single Majorana edge mode, the SDOS has an anomalous orientational dependence on the Zeeman magnetic field. We reveal that the SDOS with a zero-energy peak is robust against the magnetic field in a certain applied direction.

We also study the topological nature of the Majorana edge mode. The ABSs found here are topologically stable against a small deformation of the Hamiltonian if the deformation preserves the time-reversal invariance and the translation invariance along the direction parallel to the edge. We introduce a topological invariant ensuring the existence of the zero-energy ABS and clarify the relevance to the number of Majorana edge modes. It is revealed that the absolute value of the topological number equals the number of the Majorana edge modes.

The organization of the present paper is as follows. In Sec. II, we introduce the Hamiltonian and the lattice Green's function formalism. In Sec. III, the results of the numerical calculations of SDOS, topological invariant, and SDOS in the presence of a Zeeman magnetic field are discussed. In Sec. IV, the conclusions and outlook are presented.

## II. FORMULATION

In this paper, we consider a two-dimensional square lattice with a Rashba-type spin-orbit coupling. The model Hamiltonian is given by

$$\begin{aligned} \mathcal{H}_0 = & \sum_{k\sigma} \varepsilon_k c_{k\sigma}^\dagger c_{k\sigma} + \lambda \sum_{\mathbf{k}} \mathbf{g}(\mathbf{k}) \cdot \hat{\sigma}_{\sigma\sigma'} c_{k\sigma}^\dagger c_{k\sigma'} \\ & + \frac{1}{2} \sum_{\mathbf{k}} [\Delta_{\sigma\sigma'}(\mathbf{k}) c_{k\sigma}^\dagger c_{-k\sigma'}^\dagger + \text{H.c.}] \\ & - \mu_B \sum_{k\sigma\sigma'} \mathbf{H} \cdot \hat{\sigma}_{\sigma\sigma'} c_{k\sigma}^\dagger c_{k\sigma'}, \end{aligned} \quad (1)$$

where  $c_{k\sigma}$  ( $c_{k\sigma}^\dagger$ ) is an annihilation (creation) operator for an electron,  $\hat{\sigma}$  and  $\hat{\sigma}_i$  the Pauli matrices, and  $\varepsilon_k$  the energy dispersion of the electron on the square lattice,  $\varepsilon_k = -2t(\cos k_x + \cos k_y) - \mu$ , with the nearest neighbor hopping  $t$  and the chemical potential  $\mu$ . The second term is the Rashba spin-orbit coupling,  $\mathbf{g}(\mathbf{k}) = (\sin k_y, -\sin k_x, 0)$ , and the third one is the pair potential,  $\hat{\Delta}_k = i\psi(\mathbf{k})\hat{\sigma}_y + i\mathbf{d}(\mathbf{k}) \cdot \hat{\sigma}\hat{\sigma}_y$ . It is noted that superconductivity of CePt<sub>3</sub>Si has been discussed based on a tight-binding model like Eq. (1) by properly choosing the dispersion of the energy band.<sup>8</sup> In the presence of the Rashba

spin-orbit coupling, the Fermi surfaces are split into two, and we suppose intraband pairings in each spin-split bands. Then the  $\mathbf{d}$ -vector of the pairing function for triplet pairings  $\mathbf{d}(\mathbf{k})$  is aligned with the polarization vector of the Rashba spin-orbit coupling,  $\mathbf{d}(\mathbf{k}) \parallel \mathbf{g}(\mathbf{k})$ .<sup>6</sup> As a result, the triplet component of the energy gap function is given by  $\mathbf{d}(\mathbf{k}) = \Delta_t f(\mathbf{k})\mathbf{g}(\mathbf{k})$ , while that of the singlet component reads  $\psi(\mathbf{k}) = \Delta_s f(\mathbf{k})$ . Here  $f(\mathbf{k})$  is given by  $f(\mathbf{k}) = 1, \sin k_x \sin k_y$ , and  $(\cos k_x - \cos k_y)$  for the  $s + p, d_{xy} + p$ , and  $d_{x^2-y^2} + f$ -wave, respectively.<sup>35</sup> We also introduce the Zeeman splitting term in an applied magnetic field  $\mu_B \mathbf{H}$  for later use. From our Hamiltonian, we have the following retarded Green's function in the infinite system:

$$[\check{G}^{0R}(\mathbf{k}, \omega)]^{-1} = (\omega + i\eta)\check{I}_{4 \times 4} - \check{\mathcal{H}}(\mathbf{k}), \quad (2)$$

with

$$\check{\mathcal{H}}(\mathbf{k}) = \begin{pmatrix} \hat{\xi}_k & \hat{\Delta}_k \\ \hat{\Delta}_k^\dagger & -\hat{\xi}_{-k}^* \end{pmatrix}, \quad (3)$$

where  $\hat{\xi}_k = \varepsilon_k \hat{I}_{2 \times 2} + \lambda \mathbf{g}(\mathbf{k}) \cdot \hat{\sigma} - \mu_B \mathbf{H} \cdot \hat{\sigma}$  with the  $4 \times 4$  ( $2 \times 2$ ) unit matrix  $\check{I}_{4 \times 4}$  ( $\hat{I}_{2 \times 2}$ ).

To calculate SDOS, we construct the Green's function in a semi-infinite system. In the actual numerical calculation, we use the periodic boundary condition along the  $x$  direction with a sufficiently large size of mesh. To prepare the (100) surface at  $x = a_0$ , we introduce vacuum layers on the right side of the  $x = a_0$  site as shown in Fig. 1. Here it is sufficient to introduce the two vacuum layers since there is no long-range hopping or long-range pairing over three lattice constants in the present model. On the vacuum layers, we add the following term to the Hamiltonian:

$$\mathcal{H}' = V \sum_{x_i=a_1, a_2} \sum_{\sigma} n_{i\sigma}, \quad (4)$$

where  $n_{i\sigma} = c_{i\sigma}^\dagger c_{i\sigma}$  is a number operator at site  $i$  with spin  $\sigma$ , and  $V$  is the on-site potential. In the limit  $V \rightarrow \infty$ , no electron exists on the vacuum layers.

The Green's function in the presence of infinite potential barriers is obtained by using the T-matrix method.<sup>36</sup> First, we switch on the potential  $V$  only at the site  $x = a_1$ . The

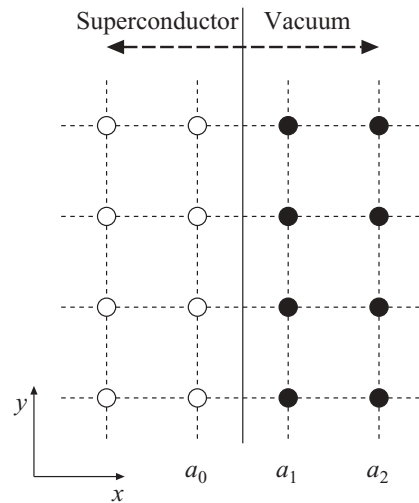


FIG. 1. (100) surface of square lattice. White and black circles show the sites without and with potential  $V$ , respectively.

Green's function  $\check{G}^{1R}(x_1, x_2; k_y, \omega)$  in this situation satisfies the following equation:

$$\check{G}^{1R}(x_1, x_2; k_y, \omega) = \check{G}^{0R}(x_1, x_2; k_y, \omega) + \check{G}^{0R}(x_1, a_1; k_y, \omega) V \check{\tau}_3 \check{G}^{1R}(a_1, x_2; k_y, \omega), \quad (5)$$

where  $\check{G}^{0R}(x_1, x_2; k_y, \omega)$  is the Fourier component  $\check{G}^{0R}(\mathbf{k}, \omega)$  with respect to  $k_x$ :

$$\check{G}^{0R}(x_1, x_2; k_y, \omega) = \frac{1}{N_x} \sum_{k_x} \check{G}^{0R}(\mathbf{k}, \omega) e^{ik_x(x_1 - x_2)}. \quad (6)$$

Here  $N_x$  is the number of  $x$ -meshes, and  $\check{\tau}_3$  is the Pauli matrix in the particle-hole space:

$$\check{\tau}_3 = \begin{pmatrix} \hat{I}_{2 \times 2} & 0 \\ 0 & -\hat{I}_{2 \times 2} \end{pmatrix}. \quad (7)$$

In the  $V \rightarrow \infty$  limit, we have the following solution of Eq. (5):

$$\check{G}^{1R}(x_1, x_2; k_y, \omega) = \check{G}^{0R}(x_1, x_2; k_y, \omega) - \check{G}^{0R}(x_1, a_1; k_y, \omega) [\check{G}^{0R}(a_1, a_1; k_y, \omega)]^{-1} \times \check{G}^{0R}(a_1, x_2; k_y, \omega). \quad (8)$$

Then we switch on the potential  $V$  at the site  $x = a_2$  as well. For the Green's function  $\check{G}^{2R}(x_1, x_2; k_y, \omega)$  in this case, we have the following equation:

$$\check{G}^{2R}(x_1, x_2; k_y, \omega) = \check{G}^{1R}(x_1, x_2; k_y, \omega) + \check{G}^{1R}(x_1, a_2; k_y, \omega) V \check{\tau}_3 \check{G}^{1R}(a_2, x_2; k_y, \omega). \quad (9)$$

Therefore, taking the  $V \rightarrow \infty$  limit, we obtain the Green's function in the semi-infinite system:

$$\check{G}^{2R}(x_1, x_2; k_y, \omega) = \check{G}^{1R}(x_1, x_2; k_y, \omega) - \check{G}^{1R}(x_1, a_2; k_y, \omega) [\check{G}^{1R}(a_2, a_2; k_y, \omega)]^{-1} \times \check{G}^{1R}(a_2, x_2; k_y, \omega). \quad (10)$$

From (8) and (10), we can calculate the SDOS  $\rho_s(\omega)$ , which is given by the local density of states at  $x = a_0$ :

$$\rho_s(\omega) = -\frac{1}{N_y} \sum_{k_y} \sum_{\alpha=1,2} \text{Im}[G_{\alpha\alpha}^{2R}(a_0, a_0; k_y, \omega)], \quad (11)$$

while the DOS in the bulk is given by

$$\rho_b(\omega) = -\frac{1}{N_x N_y} \sum_{k_x, k_y} \sum_{\alpha=1,2} \text{Im}[G_{\alpha\alpha}^{0R}(\mathbf{k}, \omega)], \quad (12)$$

where  $N_x$  and  $N_y$  are the number of meshes along the  $x$  and  $y$  directions, respectively. In the calculation presented in the following, we choose  $N_x = N_y = 2^{13}$ . We set  $t = \Delta_0 = 1$  for the unit of energy. The number of electrons per unit cell is 0.3 ( $\mu \sim -2.40t$ ). To guarantee the convergence, we use  $\eta = 0.03t$  for the infinitesimal imaginary parts in Eq. (2).

### III. RESULTS

In this section, we first focus on the local density of state at the surface, i.e., SDOS  $\rho_s(\omega)$  for various pairing symmetry.

Since spin-singlet and spin-triplet components of pair potential mix in general, we introduce a parameter  $r_s$ , which denotes the ratio of the singlet component. The parameter  $r_s$  ( $0 \leq r_s \leq 1$ ) is defined as  $\Delta_s = r_s \Delta_0$  and  $\Delta_t = (1 - r_s) \Delta_0$ .

The SDOS for the  $s + p$ -wave case is plotted in Fig. 2. In this case, the bulk DOS  $\rho_b(\omega)$  always has a  $U$ -shaped gap structure, as shown by the solid lines. The magnitude of the gap is given by  $|\Delta_s - \Delta_t|$ . For  $\Delta_s > \Delta_t$ , the SDOS  $\rho_s(\omega)$  also has a  $U$ -shaped gap structure, as shown in the dashed lines in Figs. 2(a) and 2(b). On the other hand, for  $\Delta_t > \Delta_s$  with  $r_s = 0.2$  and  $r_s = 0$ , the resulting  $\rho_s(\omega)$  has a residual value at  $\omega = 0$  as shown in Figs. 2(c) and 2(d). To elucidate the origin of the residual SDOS in the bulk energy gap, we also show the angle-resolved surface density of states (ARSDOS)  $-(1/\pi) \sum_{\alpha=1,2} \text{Im}[G_{\alpha\alpha}^{2R}(a_0, a_0; k_y, \omega)]$ . As shown in Fig. 3(a), ARSDOS shows a full gap structure without any inner gap state for a singlet dominant case ( $\Delta_s > \Delta_t$ ). On the other hand, as shown in Fig. 3(b), the ARSDOS for a triplet dominant case ( $\Delta_t > \Delta_s$ ) has two branches of ABS, which are dubbed helical edge modes.<sup>13,14</sup> The presence of helical edge modes inside the bulk energy gap induces the residual SDOS inside the bulk energy gap.

Next we look at SDOS for the  $d_{x^2-y^2} + f$ -wave case plotted in Fig. 4. In this case,  $\rho_b(\omega)$  always has a  $V$ -shaped gap structure as shown by the solid lines reflecting the nodal structures of the bulk energy gap. The corresponding  $\rho_s(\omega)$  (dashed line) also has a similar  $V$ -shaped gap structure for the singlet dominant case ( $\Delta_s > \Delta_t$ ) with  $r_s = 1$  and  $r_s = 0.8$ . As shown in Fig. 5(a), there is no inner gap state in ARSDOS, while the bulk energy gap has a strong  $k_y$  dependence. On the other hand, for the triplet dominant case ( $\Delta_t > \Delta_s$ ) with  $r_s = 0.2$  and  $r_s = 0$ ,  $\rho_s(\omega)$  has two additional peaks as shown by the dashed lines in Figs. 4(c) and 4(d) as compared to the bulk density of states<sup>18</sup> (solid lines). The additional two peaks in the SDOS originate from the helical edge modes generated inside the energy gap as shown in Fig. 5(b).<sup>18</sup>

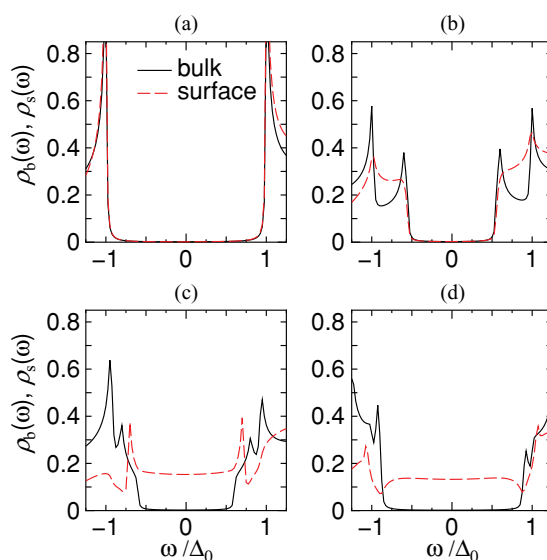


FIG. 2. (Color online) Local density of states for a  $s + p$ -wave in the bulk (solid lines) and at the surface (dashed lines) for  $\lambda = 0.5$  and  $r_s = 1.0, 0.8, 0.2$ , and  $0.0$ .

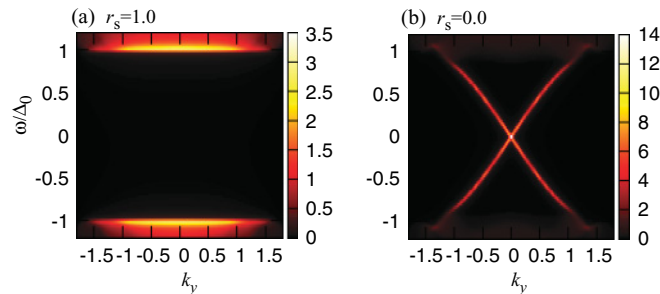


FIG. 3. (Color online) Angle-resolved local density of state of  $s + p$ -wave pairing is plotted as a function of  $k_y$  with  $\lambda = 0.5$ . (a)  $\Delta_s = \Delta_0$  and  $\Delta_t = 0$ , (b)  $\Delta_t = \Delta_0$  and  $\Delta_s = 0$ .

The SDOS for  $d_{xy} + p$ -wave NCS superconductors is plotted in Figs. 6 and 8. In this case,  $\rho_s(\omega)$  has very different line shapes as compared to the former two cases. In particular, for the spin-triplet dominant pairing, we find that the SDOS is very sensitive to the spin-orbit coupling. To show this, we first start with the case without spin-orbit coupling, i.e.,  $\lambda = 0$  (see Fig. 6).  $\rho_b(\omega)$  has a V-shaped gap structure as shown by the solid lines, reflecting the nodal structure of pair potential. The corresponding  $\rho_s(\omega)$  (dashed line) has a zero-energy peak (ZEP) for the singlet dominant case with  $r_s = 1$  and  $r_s = 0.8$ . This ZEP comes from the midgap ABS with a flat dispersion as shown in Fig. 7(a), and it is essentially the same as that appears in the surface state of the high- $T_c$  cuprate.<sup>20,21</sup> On the other hand, for the triplet dominant case with  $r_s = 0.2$  and  $r_s = 0$ , the ZEP disappears, but  $\rho_s(\omega)$  supports two additional peaks instead, as shown by the dashed lines in Figs. 6(c) and 6(d), respectively. The additional two peaks are generated by the anomalous ABS. In the absence of Rashba spin-orbit coupling, the dispersion of the anomalous ABS for a  $d_{xy} + p$ -wave pairing is very similar to the helical edge modes for a  $d_{x^2-y^2} + f$ -wave pairing, as shown in Fig. 7(b). However, the intensity of ARSDOS near  $k_y \sim 0$  is very low

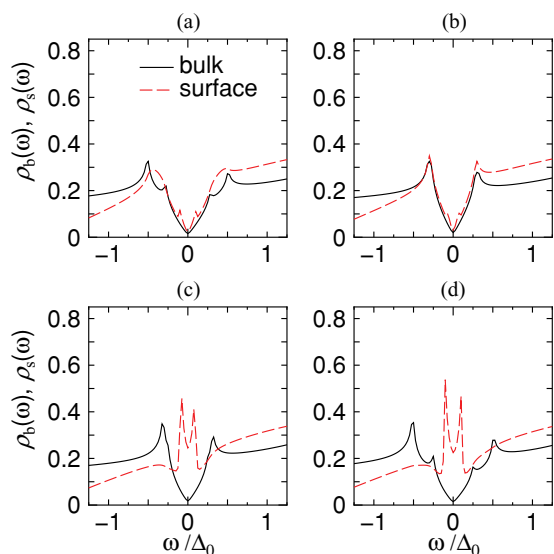


FIG. 4. (Color online) Local density of states for  $d_{x^2-y^2} + f$ -wave in the bulk (solid lines) and at the surface (dashed lines) for  $\lambda = 0.5$  and  $r_s = 1.0, 0.8, 0.2$ , and  $0.0$ .

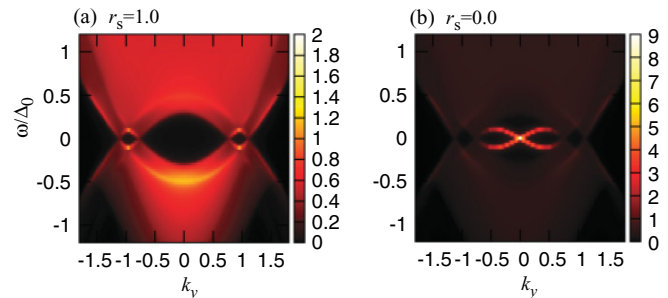


FIG. 5. (Color online) Angle-resolved local density of state of  $d_{x^2-y^2} + f$ -wave pairing is plotted as a function of  $k_y$  with  $\lambda = 0.5$ . (a)  $\Delta_s = \Delta_0$  and  $\Delta_t = 0$ , (b)  $\Delta_t = \Delta_0$  and  $\Delta_s = 0$ .

since the magnitude of the excitation energy of the ABS is close to the bulk energy gap. In the two-dimensional free-electron model for the NCS superconductor, it has been shown that the dispersion of the ABS corresponds to the bulk energy gap, and the intensity of ARSDOS is completely absent for  $|k_y| < k_c$ , where  $k_c$  is a certain critical wave number.<sup>18</sup> Thus, in contrast to the helical edge mode in the  $d_{x^2-y^2} + f$ -wave pairing case, the values of the SDOS for  $d_{xy} + p$ -wave pairing at  $\omega/\Delta = 0$  are very close to zero.

Let us now consider the  $d_{xy} + p$ -wave case with nonzero spin-orbit coupling  $\lambda$ . As shown in Fig. 8, the bulk DOS  $\rho_b(\omega)$  shows a V-shaped gap structure similar to Fig. 6. Then, for the singlet dominant case with  $r_s = 1$  and  $r_s = 0.8$ , the SDOS  $\rho_s(\omega)$  [dashed line in Figs. 8(a) and 8(b)] has a ZEP similar to Figs. 6(a) and 6(b). On the other hand, for the triplet dominant case with  $r_s = 0.2$  and  $r_s = 0$ , in addition to the two peaks similar to those in Figs. 6(c) and 6(d), ZEP appears as shown in Figs. 8(c) and 8(d). It is remarkable that ZEP is generated by spin-orbit coupling  $\lambda$ .<sup>18</sup>

To show this new type of ZEP much more clearly, we plot ARSDOS of the  $d_{xy} + p$ -wave case in Fig. 9 with

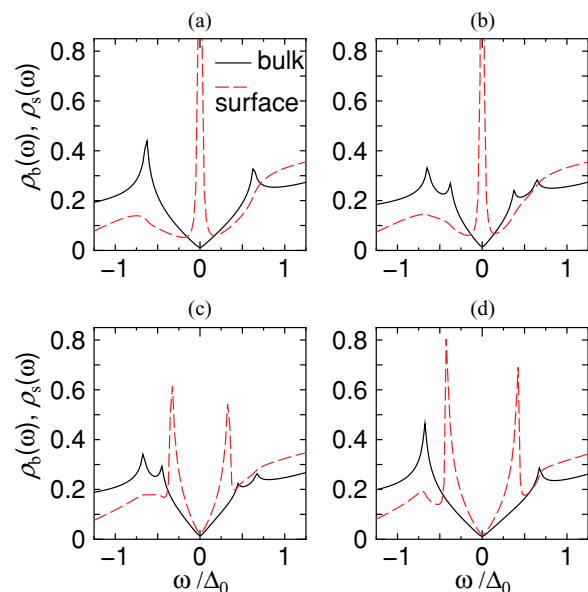


FIG. 6. (Color online) Local density of states for  $d_{xy} + p$ -wave in the bulk (solid lines) and at the surface (dashed lines) for  $\lambda = 0.0$  and  $r_s = 1.0, 0.8, 0.2$ , and  $0.0$ .

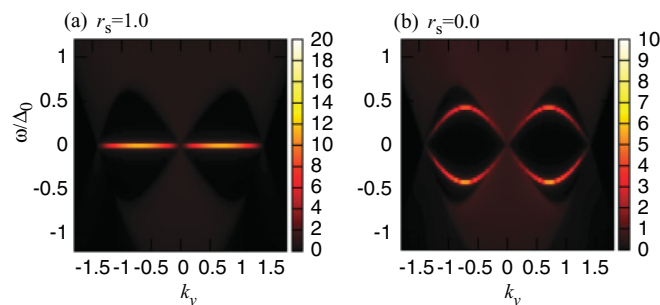


FIG. 7. (Color online) Angle-resolved local density of state of  $d_{xy} + p$ -wave pairing is plotted as a function of  $k_y$  with  $\lambda = 0.0$ . (a)  $\Delta_s = \Delta_0$  and  $\Delta_t = 0$ , (b)  $\Delta_t = \Delta_0$  and  $\Delta_s = 0$ .

$\lambda = 0.5$ . Comparing with the ARSDOS in Fig. 7, for the triplet dominant case, we find that an additional zero-energy state (ZES) appears. In the presence of the spin-orbit coupling, the Fermi surface is split into the large one with the Fermi momentum  $k_2$  and the small one with  $k_1$ . The ZES exists only for  $k_y$  between the split Fermi surfaces, namely, for  $k_y$  with  $k_2 > |k_y| > k_1$ . It can be shown that the Bogoliubov quasiparticle creation operator  $\gamma_{k_y}^\dagger$  for the ZES at  $x = a_0$  satisfies  $\gamma_{k_y}^\dagger = \gamma_{-k_y}$ .<sup>18</sup> Then the local quasiparticle creation operator  $\psi(y) = \frac{1}{N_y} \sum_{k_y} \gamma_{k_y} e^{ik_y y}$  satisfies the Majorana condition  $\psi(y) = \psi^\dagger(y)$ . Therefore, the ZES is identified as a Majorana fermion.

For singlet-dominant  $d_{xy} + p$ -wave NCS superconductors, we obtain the SDOS and ARSDOS depicted in Figs. 8(a) and 8(b) and Fig. 9(a), respectively. At first sight, they look very similar to those in Figs. 6(a) and 6(b) and Fig. 7(a). However, for  $k_y$  with  $k_2 > |k_y| > k_1$ , we again have a single branch of a ZES on the edge. As is shown later, because of the existence of the time-reversal invariant Majorana fermion (TRIMF), the

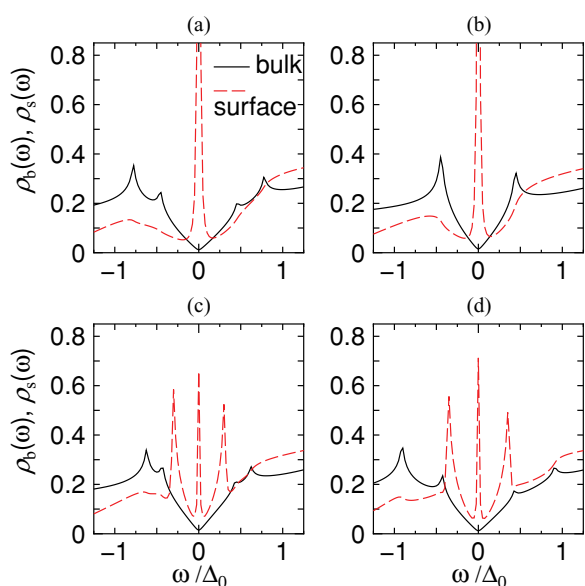


FIG. 8. (Color online) Local density of states for  $d_{xy} + p$ -wave in the bulk (solid lines) and at the surface (dashed lines) for  $\lambda = 0.5$  and  $r_s = 1.0, 0.8, 0.2$ , and  $0.0$ .

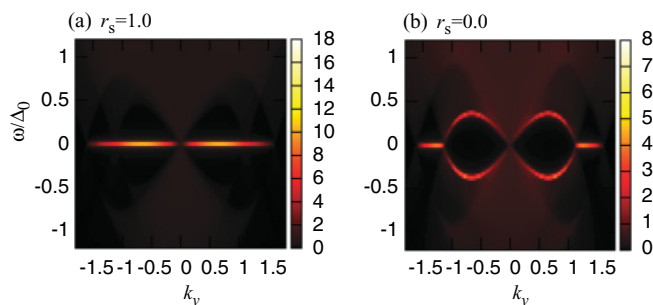


FIG. 9. (Color online) Angle-resolved local density of state of  $d_{xy} + p$ -wave pairing is plotted as a function of  $k_y$  with  $\lambda = 0.5$ . (a)  $\Delta_s = \Delta_0$  and  $\Delta_t = 0$ , (b)  $\Delta_t = \Delta_0$  and  $\Delta_s = 0$ .

SDOS for the  $d_{xy} + p$ -wave NCS superconductor shows a peculiar dependence on the Zeeman magnetic field.

Unlike the Majorana fermions studied before, the present Majorana fermion is realized with the time-reversal invariance. The TRIMF has the following three characteristics: (1) It has a unique flat dispersion. To be consistent with the time-reversal invariance, the single branch of ZES should be symmetric under  $k_y \rightarrow -k_y$ . Therefore, by taking into account the particle-hole symmetry as well, the flat dispersion is required. On the other hand, the conventional time-reversal breaking Majorana edge state has a linear dispersion. (2) The spin-orbit coupling is indispensable for the existence of the TRIMF. Without the spin-orbit coupling, the TRIMF vanishes. (3) The TRIMF is topologically stable under a small deformation of the Hamiltonian. The topological stability is ensured by a topological number, which we will show shortly. Furthermore, we notice that the flat dispersion is terminated at nodes of the bulk gap. This is because the topological number can change at  $|k_y| = k_i$  ( $i = 1, 2$ ) where the bulk gap closes.

To see the topological nature of the TRIMF, we start from the Bogoliubov-de Gennes (BdG) Hamiltonian in the bulk system defined in Eq. (3) without a Zeeman magnetic field. In the Nambu representation, the BdG Hamiltonian (3) has the particle-hole symmetry:

$$\check{C}\check{\mathcal{H}}(\mathbf{k})\check{C}^\dagger = -\check{\mathcal{H}}^*(-\mathbf{k}), \quad \check{C} = \begin{pmatrix} 0 & \hat{I}_{2 \times 2} \\ \hat{I}_{2 \times 2} & 0 \end{pmatrix}. \quad (13)$$

In addition, from the time-reversal invariance, the BdG Hamiltonian satisfies

$$\check{\Theta}\check{\mathcal{H}}(\mathbf{k})\check{\Theta}^\dagger = \check{\mathcal{H}}^*(-\mathbf{k}), \quad \check{\Theta} = \begin{pmatrix} i\sigma_y & 0 \\ 0 & i\sigma_y \end{pmatrix}. \quad (14)$$

Therefore, we can define the operator  $\Gamma$ , which anticommutes with the BdG Hamiltonian:<sup>29</sup>

$$\{\check{\mathcal{H}}(\mathbf{k}), \check{\Gamma}\}_+ = 0. \quad (15)$$

Here  $\Gamma$  is defined as the product of particle-hole transformation operator  $C$  and time-reversal operator  $\Theta$ :

$$\check{\Gamma} = -i\check{C}\check{\Theta} = \begin{pmatrix} 0 & \hat{\sigma}_y \\ \hat{\sigma}_y & 0 \end{pmatrix}. \quad (16)$$

Now we take the basis that diagonalizes  $\check{\Gamma}$

$$\check{U}_\Gamma^\dagger \check{\Gamma} \check{U}_\Gamma = \begin{pmatrix} \hat{I}_{2 \times 2} & 0 \\ 0 & -\hat{I}_{2 \times 2} \end{pmatrix} \quad (17)$$

with the unitary matrix  $\check{U}_\Gamma$

$$\check{U}_\Gamma = \check{U}_\Gamma^\dagger = \frac{1}{\sqrt{2}} \begin{pmatrix} \hat{I}_{2 \times 2} & \hat{\sigma}_y \\ \hat{\sigma}_y & -\hat{I}_{2 \times 2} \end{pmatrix}. \quad (18)$$

Then we find that the BdG Hamiltonian  $\check{\mathcal{H}}(\mathbf{k})$  becomes off-diagonal in this basis:

$$\check{U}_\Gamma^\dagger \check{\mathcal{H}}(\mathbf{k}) \check{U}_\Gamma = \begin{pmatrix} 0 & \hat{q}(\mathbf{k}) \\ \hat{q}(\mathbf{k})^\dagger & 0 \end{pmatrix}, \quad (19)$$

where  $\hat{q}(\mathbf{k}) = \hat{\xi}_k \hat{\sigma}_y - \hat{\Delta}_k$ .

To classify the existence or nonexistence of the ZES with  $k_y = k_y^0$ , we change  $k_x$  from  $-\pi$  to  $\pi$  for a fixed value of  $k_y = k_y^0$ . The winding number  $W$  is defined as a number of revolutions of  $\det\{\hat{q}(\mathbf{k})\} \equiv m_1(\mathbf{k}) + im_2(\mathbf{k})$  around the origin of complex plane when  $k_x$  changes from  $-\pi$  to  $\pi$ :

$$W(k_y^0) = \frac{1}{2\pi} \int_{-\pi}^{\pi} \frac{\partial \theta(\mathbf{k})}{\partial k_x} \Big|_{k_y \rightarrow k_y^0} dk_x, \quad (20)$$

with  $\theta(\mathbf{k}) \equiv \arg \det\{\hat{q}(\mathbf{k})\} = \tan^{-1}(m_2(\mathbf{k})/m_1(\mathbf{k}))$ . The resulting  $W(k_y^0)$  must be an integer since the starting point and the end point of integration route are equivalent in the Brillouin zone. Therefore, the value of  $W(k_y^0)$  changes discretely with the change of  $k_y$  value. When the gap of the system closes at certain points on the integration route,  $W(k_y^0)$  is ill defined since  $\det\{\hat{q}(\mathbf{k})\}$  becomes zero on such points. Thus, the value of  $W(k_y)$  does not change by the small change of  $k_y$  value unless the energy gap closes.

Here we study the winding number for the  $d_{xy} + p$ -wave NCS superconductors for the two trajectories at  $k_y = 0.20\pi$  and  $0.45\pi$  as shown in Fig. 10. For  $k_y = 0.20\pi$ , the trajectory crosses the Fermi surfaces four times. On the other hand, for  $k_y = 0.45\pi$ , it crosses two times. As we have explained, the winding number  $W(k_y)$  does not change unless the energy gap closes. For  $d_{xy} + p$ -wave pairings, the energy gap closes at  $(\pm k_1, 0)$ ,  $(\pm k_2, 0)$ ,  $(0, \pm k_1)$ , and  $(0, \pm k_2)$ . Therefore,  $W(k_y)$  can change only at  $k_y = \pm k_1$ ,  $k_y = \pm k_2$ , or  $k_y = 0$ . Thus, it is sufficient to study the representative point in each  $k_y$  range.

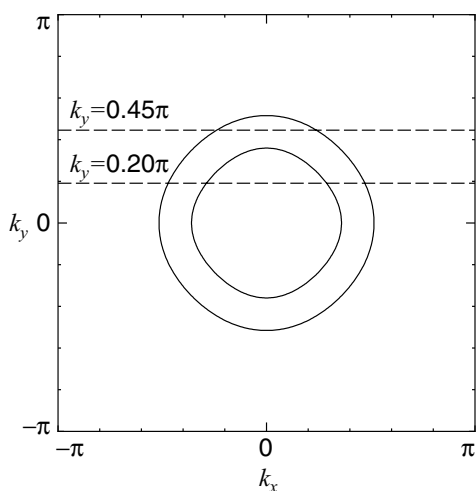


FIG. 10. Fermi surfaces of spin-split bands due to the Rashba spin-orbit coupling (solid lines) and cutting lines  $k_y = 0.20\pi$  and  $0.45\pi$  (dashed lines).

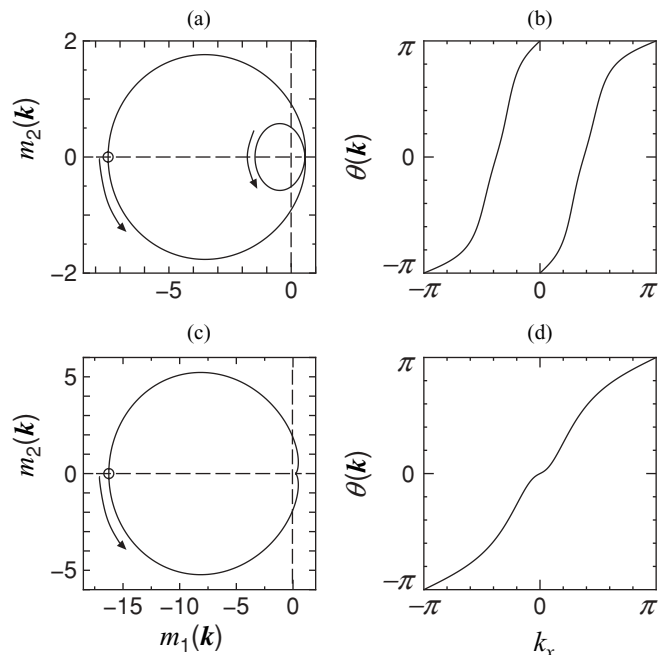


FIG. 11. Polar plot of  $\theta(\mathbf{k})$  for  $\Delta_s = \Delta_0$  and  $\Delta_t = 0$  as a function of  $k_x$  with fixed  $k_y$  for a  $d_{xy} + p$ -wave NCS superconductor. (a)  $k_y = 0.2\pi$  and (c)  $k_y = 0.45\pi$ . The white circle corresponds to  $k_x = \pm\pi$ , and arrows show the direction in which the values of  $k_x$  increase. The corresponding  $\theta = \tan^{-1}(m_2/m_1)$  is plotted as a function of  $k_x$  for (b)  $k_y = 0.2\pi$  and (d)  $k_y = 0.45\pi$ .

We first focus on the singlet dominant  $d_{xy} + p$ -wave NCS superconductor with  $\Delta_s = \Delta_0$  and  $\Delta_t = 0$ . For  $k_y = 0.2\pi$ , as shown in Fig. 11(a),  $m_1$  and  $m_2$  draw a curve that turns anticlockwise twice around the  $(m_1, m_2) = (0, 0)$  if we change  $k_x$  from  $-\pi$  to  $\pi$ . At the same time,  $\theta(\mathbf{k})$  changes twice from  $-\pi$  to  $\pi$  as shown in Fig. 11(b). Therefore, the resulting winding number  $W$  is  $W = 2$ . On the other hand, for  $k_y = 0.45\pi$ ,  $m_1$  and  $m_2$  draw a curve that turns anticlockwise once around the  $(m_1, m_2) = (0, 0)$  as shown in Fig. 11(c). Moreover,  $\theta(\mathbf{k})$  changes once from  $-\pi$  to  $\pi$  as shown in Fig. 11(d). Thus, the resulting winding number  $W$  equals 1. This means that these two cases belong to different topological classes. In a similar manner, it is possible to generalize our argument for other  $k_y$ 's ( $-\pi < k_y < \pi$ ). We summarize the obtained results in Table I(a).

The same plot of  $m_i(\mathbf{k})$  and  $\theta(\mathbf{k})$  for the triplet dominant  $d_{xy} + p$ -wave NCS superconductors with  $\Delta_t = \Delta_0$  and  $\Delta_s = 0$  is shown in Fig. 12. For  $k_y = 0.2\pi$ ,  $m_1$  and  $m_2$  draw a curve as shown in Fig. 12(a). However, it does not turn around the point  $(m_1, m_2) = (0, 0)$  with the change of  $k_x$  from  $-\pi$  to  $\pi$ . At the same time,  $\theta(\mathbf{k})$  does not change from  $-\pi$  to  $\pi$  as shown in Fig. 12(b), in contrast to that in Fig. 11(b). This corresponds to the fact that the resulting winding number  $W$  equals 0. On the other hand, for  $k_y = 0.45\pi$ ,  $m_1$  and  $m_2$  draw a curve that turns clockwise once around the  $(m_1, m_2) = (0, 0)$  as shown in Fig. 12(c). Also,  $\theta(\mathbf{k})$  changes once from  $\pi$  to  $-\pi$  as shown in Fig. 12(d). Therefore, the corresponding winding number  $W$  equals  $-1$ . In a manner similar to the singlet dominant case, it is possible to generalize this argument for other

TABLE I. The winding number  $W(k_y)$  for  $d_{xy} + p$ -wave with (a)  $\Delta_s > \Delta_t$ , (b)  $\Delta_t > \Delta_s$ .

	$k_y$	$k_y > k_2$	$k_2 > k_y > k_1$	$k_1 > k_y > 0$	$0 > k_y > -k_1$	$-k_1 > k_y > -k_2$	$-k_2 > k_y$
(a)	$W(k_y)$	0	1	2	-2	-1	0
(b)	$W(k_y)$	0	-1	0	0	1	0

$k_y$  ( $-\pi < k_y < \pi$ ). The obtained results are summarized in Table I(b).

Comparing the obtained winding number  $W(k_y)$  in Table I with the ARSDOS in Fig. 9, we notice that zero-energy ABS appears only for  $k_y$  with nonzero  $W(k_y)$ . This correspondence implies that the existence and the stability of the zero-energy ABS is ensured by the winding number. Indeed, we can say that the absolute value of  $W$ , i.e.,  $|W|$  equals the number of branches of zero-energy ABS.<sup>37</sup> In other words, the number of TRIMFs equals the absolute value of  $W$ . Furthermore, the TRIMFs found here are topologically stable against a small deformation of the BdG Hamiltonian if the deformation preserves the time-reversal invariance and the translation invariance along the direction parallel to the edge, both of which are necessary to define the winding number. It should be remarked that for both the singlet dominant case and the triplet dominant one, a single TRIMF is generated for  $k_2 > |k_y| > k_1$ .

As we have shown, the time-reversal invariance is essential to define the winding number  $W$  ensuring the topological stability of the TRIMF. Therefore, in general, if we apply a perturbation breaking the time-reversal invariance, the winding number  $W$  becomes meaningless. In other words, a time-

reversal breaking perturbation may change the SDOS of the TRIMF substantially.

As a time-reversal breaking perturbation, we consider the Zeeman magnetic field. Let us look at the SDOS in the presence of Zeeman magnetic field  $\mathbf{H}$ . First, we consider the singlet dominant  $d_{xy} + p$ -wave NCS superconductor. Without the spin-orbit coupling, the ABS becomes conventional and can be expressed by double TRIMFs. In this case, as we expected, it is found that the ZEP of SDOS from the double TRIMFs is split in two by any Zeeman magnetic field  $\mathbf{H}$  as shown in Fig. 13.<sup>38</sup> It is also noted that the resulting SDOS is independent of the direction of  $\mathbf{H}$  due to the spin-rotational symmetry in the system. Thus, the SDOSs  $\rho_s(\omega)$  for  $\mu_B H_x = 0.1t$  ( $\mathbf{H} \parallel \mathbf{x}$ ),  $\mu_B H_y = 0.1t$  ( $\mathbf{H} \parallel \mathbf{y}$ ) and  $\mu_B H_z = 0.1t$  ( $\mathbf{H} \parallel \mathbf{z}$ ) are identical.

On the other hand, in the presence of the spin-orbit coupling, this property is not satisfied anymore. As shown in Fig. 14,  $\rho_s(\omega)$  has different structures for  $\mu_B H_x = 0.1t$  [Fig. 14(b)],  $\mu_B H_y = 0.1t$  [Fig. 14(c)], and  $\mu_B H_z = 0.1t$  [Fig. 14(d)], respectively. The orientational dependence of SDOS is due to the presence of the spin-orbit coupling since the spin-rotational symmetry is broken. It is noted that the three-peak structure including the ZEP appears for  $\mu_B H_y = 0.1t$  ( $\mathbf{H} \parallel \mathbf{y}$ ). The presence of the ZEP against the Zeeman magnetic field along the edge, which is  $H_y$  in this case, is relevant to the existence of the single Majorana edge mode with zero energy at  $k_2 > |k_y| > k_1$  as shown in Fig. 15(b). This Majorana edge mode has a dispersion with nonzero energy when the Zeeman magnetic field is applied along the  $x$  direction [Fig. 15(a)]. On the other hand, the double TRIMFs at  $|k_y| < k_1$  are split in two for any direction of the Zeeman magnetic field. We have checked that the height of ZEP  $\rho_s(0)$  drastically decreases even if ZEP remains for  $\mu_B H_y = 0.1t$  ( $\mathbf{H} \parallel \mathbf{y}$ ).

Next we consider the triplet dominant  $d_{xy} + p$ -wave NCS superconductor. For simplicity, we suppose that only the triplet component  $\Delta_t$  exists. As was shown in Fig. 9(b), in the absence of the Zeeman magnetic field, a zero-energy ABS exists, and

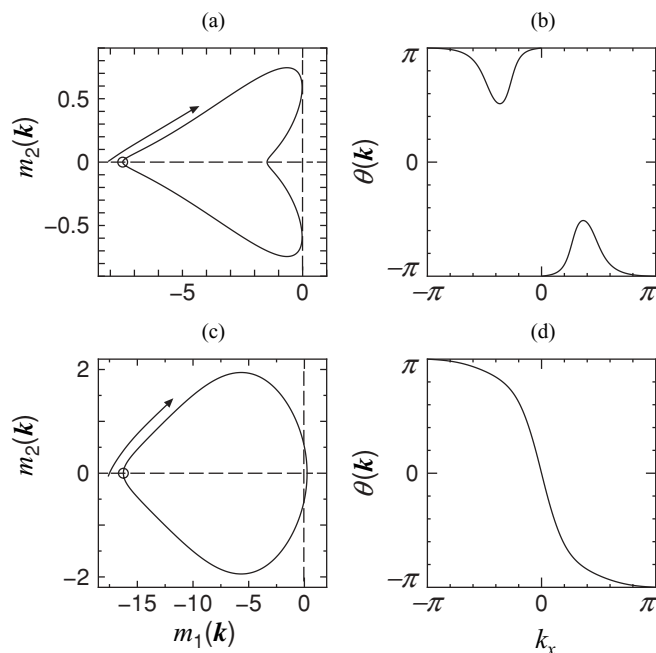


FIG. 12. Polar plot of  $\theta(\mathbf{k})$  for  $\Delta_t = \Delta_0$  and  $\Delta_s = 0$  as a function of  $k_x$  with fixed  $k_y$  for  $d_{xy} + p$ -wave NCS superconductor. (a)  $k_y = 0.2\pi$  and (c)  $k_y = 0.45\pi$ , where the white circle corresponds to  $k_x = \pm\pi$  and arrows show the direction in which the values of  $k_x$  increase. The corresponding  $\theta = \tan^{-1}(m_2/m_1)$  is plotted as a function of  $k_x$  for (b)  $k_y = 0.2\pi$  and (d)  $k_y = 0.45\pi$ .

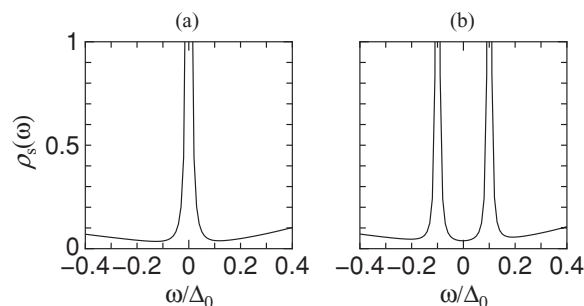


FIG. 13. Local density of states at the surface for  $d_{xy} + p$ -wave with  $\Delta_s = \Delta_0$  and  $\Delta_t = 0$  for  $\lambda = 0$  and (a)  $\mu_B \mathbf{H} = 0$ , (b)  $\mu_B H_x = 0.1$  ( $\mathbf{H} \parallel \mathbf{x}$ ).

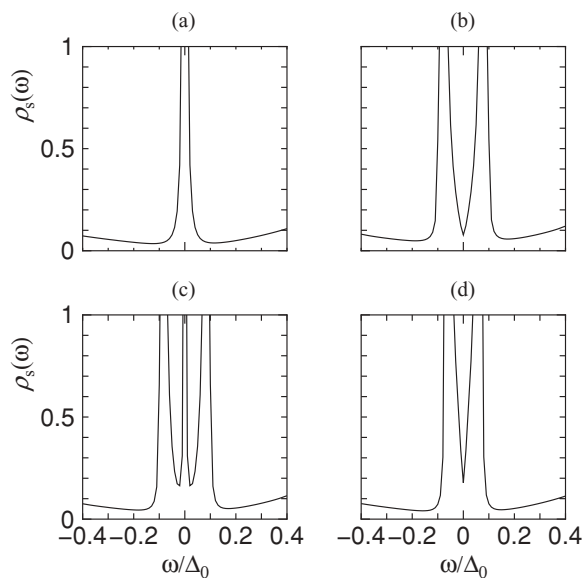


FIG. 14. Local density of states at the surface for  $d_{xy} + p$ -wave with  $\Delta_s = \Delta_0$  and  $\Delta_t = 0$  for  $\lambda = 0.5$  and (a)  $\mu_B \mathbf{H} = 0$ , (b)  $\mu_B H_x = 0.1t (\mathbf{H} \parallel \mathbf{x})$ , (c)  $\mu_B H_y = 0.1t (\mathbf{H} \parallel \mathbf{y})$ , (d)  $\mu_B H_z = 0.1t (\mathbf{H} \parallel \mathbf{z})$ .

it can be described by a single TRIMF. The resulting  $\rho_s(\omega)$  has a sharp ZEP without  $\mathbf{H}$  [Fig. 16(a)]. In a manner similar to the singlet dominant case we have described, the SDOS  $\rho_s(\omega)$  under the Zeeman magnetic field has a strong orientational dependence of  $\mathbf{H}$  as shown in Figs. 16(b), 16(c), and 16(d). It is noted that ZEP remains when the applied Zeeman field is along the  $y$  direction. This implies that the single TRIMF in the  $d_{xy} + p$ -wave NCS superconductor is robust against the Zeeman magnetic field applied in the direction along the edge.

We would like to emphasize that, as shown from these calculations, the tunneling spectroscopy with the Zeeman magnetic field is available to identify the single TRIMF in the  $d_{xy} + p$ -wave NCS superconductor. Simultaneous existence of the strong orientational dependence of the magnetic field and the robust ZEP under a certain direction of the magnetic field is strong evidence to support the single Majorana fermion in this material.

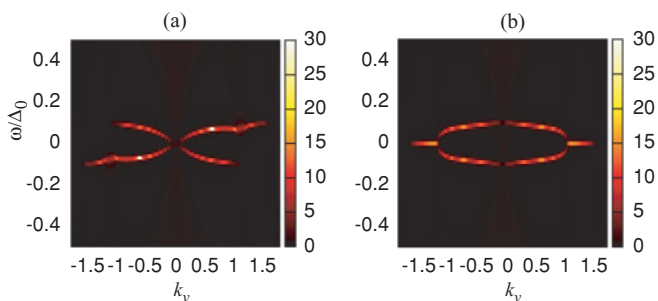


FIG. 15. (Color online) Angle-resolved local density of state for  $d_{xy} + p$ -wave pairing in the presence of the Zeeman magnetic field is plotted as a function of  $k_y$  with  $\lambda = 0.5$ ,  $\Delta_s = \Delta_0$  and  $\Delta_t = 0$ . (a)  $\mu_B H_x = 0.1t (\mathbf{H} \parallel \mathbf{x})$ , (b)  $\mu_B H_y = 0.1t (\mathbf{H} \parallel \mathbf{y})$ .

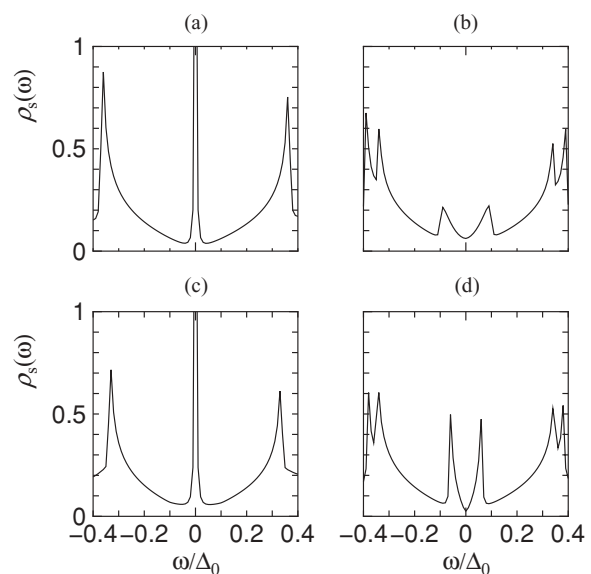


FIG. 16. Local density of states at the surface for  $d_{xy} + p$ -wave with  $\Delta_t = \Delta_0$  and  $\Delta_s = 0$  for  $\lambda = 0.5$  and (a)  $\mu_B \mathbf{H} = 0$ , (b)  $\mu_B H_x = 0.1t (\mathbf{H} \parallel \mathbf{x})$ , (c)  $\mu_B H_y = 0.1t (\mathbf{H} \parallel \mathbf{y})$ , (d)  $\mu_B H_z = 0.1t (\mathbf{H} \parallel \mathbf{z})$ .

#### IV. SUMMARY

In the present paper, we have investigated SDOS and edge modes of NCS superconductors by choosing  $s + p$ ,  $d_{x^2-y^2} + f$ , and  $d_{xy} + p$ -wave pair potential based on the lattice model Hamiltonian. For  $d_{xy} + p$ -wave pairing, an unusual ABS appears as a ZES for  $k_2 > |k_y| > k_1$  with the wavenumber parallel to the interface  $k_y$ , where  $k_1$  and  $k_2$  denote the magnitude of the Fermi wavenumber in the presence of spin-orbit coupling. The present ABS is a single Majorana edge mode preserving the time-reversal symmetry. We have defined a new type of topological invariant and clarified the relevance to the number of the time-reversal invariant Majorana edge modes. We have found that the absolute value of the topological number equals the number of the Majorana edge modes. The single Majorana edge mode is generally induced by the spin-orbit coupling. In the presence of the single Majorana edge mode, the SDOS has a strong orientational dependence of the magnetic field. In an applied magnetic field along the edge, the single Majorana edge mode is robust, and the resulting ZEP of SDOS remains. These futures may serve as a guide to detect the Majorana fermion in noncentrosymmetric superconductors by tunneling spectroscopy.

*Note added.* After our paper had been submitted, we become aware of a relevant paper.<sup>39</sup>

#### ACKNOWLEDGMENTS

This work is partly supported by the Sumitomo Foundation (MS) and the Grant-in-Aids for Scientific Research No. 22103005 (Innovative Areas “Topological Quantum Phenomena,” YT and MS), No. 20654030 (YT) and No. 22540383 (MS).

- <sup>1</sup>E. Bauer, G. Hilscher, H. Michor, C. Paul, E. W. Scheidt, A. Gribov, Y. Seropegin, H. Noël, M. Sigrist, and P. Rogl, *Phys. Rev. Lett.* **92**, 027003 (2004).
- <sup>2</sup>K. Togano, P. Badica, Y. Nakamori, S. Orimo, H. Takeya, and K. Hirata, *Phys. Rev. Lett.* **93**, 247004 (2004); M. Nishiyama, Y. Inada, and G. Q. Zheng, *Phys. Rev. B* **71**, 220505(R) (2005).
- <sup>3</sup>A. D. Hillier, J. Quintanilla, and R. Cywinski, *Phys. Rev. Lett.* **102**, 117007 (2009).
- <sup>4</sup>N. Reyren *et al.*, *Science* **317**, 1196 (2007).
- <sup>5</sup>L. P. Gor'kov and E. I. Rashba, *Phys. Rev. Lett.* **87**, 037004 (2001).
- <sup>6</sup>P. A. Frigeri, D. F. Agterberg, A. Koga, and M. Sigrist, *Phys. Rev. Lett.* **92**, 097001 (2004).
- <sup>7</sup>S. Fujimoto, *J. Phys. Soc. Jpn.* **76**, 051008 (2007).
- <sup>8</sup>Y. Yanase and M. Sigrist, *J. Phys. Soc. Jpn.* **77**, 124711 (2008); **76**, 043712 (2007).
- <sup>9</sup>Y. Tada, N. Kawakami, and S. Fujimoto, *New J. Phys.* **11**, 055070 (2009).
- <sup>10</sup>J. Linder and A. Sudbø, *Phys. Rev. B* **76**, 054511 (2007); K. Børkje and A. Sudbø, *ibid.* **74**, 054506 (2006); K. Børkje, *ibid.* **76**, 184513 (2007).
- <sup>11</sup>T. Yokoyama, Y. Tanaka, and J. Inoue, *Phys. Rev. B* **72**, 220504(R) (2005); C. Iniotakis, N. Hayashi, Y. Sawa, T. Yokoyama, U. May, Y. Tanaka, and M. Sigrist, *ibid.* **76**, 012501 (2007); M. Eschrig, C. Inotakis, and Y. Tanaka, e-print arXiv:1001.2486.
- <sup>12</sup>A. B. Vorontsov, I. Vekhter, and M. Eschrig, *Phys. Rev. Lett.* **101**, 127003 (2008).
- <sup>13</sup>Y. Tanaka, T. Yokoyama, A. V. Balatsky, and N. Nagaosa, *Phys. Rev. B* **79**, 060505(R) (2009).
- <sup>14</sup>M. Sato, *Phys. Rev. B* **73**, 214502 (2006); M. Sato and S. Fujimoto, *ibid.* **79**, 094504 (2009).
- <sup>15</sup>C. K. Lu and S. Yip, *Phys. Rev. B* **80**, 024504 (2009).
- <sup>16</sup>T. Yokoyama, S. Onari, and Y. Tanaka, *Phys. Rev. B* **75**, 172511 (2007); *J. Phys. Soc. Jpn.* **77**, 064711 (2008).
- <sup>17</sup>K. Yada, S. Onari, Y. Tanaka, J. Inoue, *Phys. Rev. B* **80**, 140509 (2009).
- <sup>18</sup>Y. Tanaka, Y. Mizuno, T. Yokoyama, K. Yada, and M. Sato, *Phys. Rev. Lett.* **105**, 097002 (2010).
- <sup>19</sup>L. J. Buchholtz and G. Zwignagl, *Phys. Rev. B* **23**, 5788 (1981); J. Hara and K. Nagai, *Prog. Theor. Phys.* **74**, 1237 (1986); S. Kashiwaya and Y. Tanaka, *Rep. Prog. Phys.* **63**, 1641 (2000).
- <sup>20</sup>C. R. Hu, *Phys. Rev. Lett.* **72**, 1526 (1994).
- <sup>21</sup>Y. Tanaka and S. Kashiwaya, *Phys. Rev. Lett.* **74**, 3451 (1995).
- <sup>22</sup>S. Kashiwaya, Y. Tanaka, M. Koyanagi, H. Takashima, and K. Kajimura, *Phys. Rev. B* **51**, 1350 (1995); S. Kashiwaya, Y. Tanaka, N. Terada, M. Koyanagi, S. Ueno, L. Alff, H. Takashima, Y. Tanuma, and K. Kajimura, *J. Phys. Chem. Solids* **59**, 2034 (1998); M. Covington, M. Aprili, E. Paraoanu, L. H. Greene, F. Xu, J. Zhu, and C. A. Mirkin, *Phys. Rev. Lett.* **79**, 277 (1997); L. Alff, H. Takashima, S. Kashiwaya, N. Terada, H. Ihara, Y. Tanaka, M. Koyanagi, and K. Kajimura, *Phys. Rev. B* **55**, R14757 (1997); J. Y. T. Wei, N.-C. Yeh, D. F. Garrigus, and M. Strasik, *Phys. Rev. Lett.* **81**, 2542 (1998); I. Iguchi, W. Wang, M. Yamazaki, Y. Tanaka, and S. Kashiwaya, *Phys. Rev. B* **62**, R6131 (2000); A. Biswas, P. Fournier, M. M. Qazilbash, V. N. Smolyaninova, H. Balcı, and R. L. Greene, *Phys. Rev. Lett.* **88**, 207004 (2002); B. Chesca, M. Seifried, T. Dahm, N. Schopohl, D. Koelle, R. Kleiner, and A. Tsukada, *Phys. Rev. B* **71**, 104504 (2005); B. Chesca, D. Doenitz, T. Dahm, R. P. Huebener, D. Koelle, R. Kleiner, Ariando, H. J. H. Smilde, and H. Hilgenkamp, *ibid.* **73**, 014529 (2006); B. Chesca, H. J. H. Smilde, and H. Hilgenkamp, *ibid.* **77**, 184510 (2008).
- <sup>23</sup>Y. Maeno, H. Hashimoto, K. Yoshida, S. Nishizaki, T. Fujita, J. G. Bednorz, and F. Lichtenberg, *Nature (London)* **372**, 532 (1994).
- <sup>24</sup>M. Matsumoto and M. Sigrist, *J. Phys. Soc. Jpn.* **68**, 994 (1999); C. Honerkamp and M. Sigrist, *J. Low Temp. Phys.* **111**, 895 (1998); M. Yamashiro, Y. Tanaka, and S. Kashiwaya, *Phys. Rev. B* **56**, 7847 (1997).
- <sup>25</sup>C. L. Kane and E. J. Mele, *Phys. Rev. Lett.* **95**, 146802 (2005); **95**, 226801 (2005); B. A. Bernevig and S. C. Zhang, *ibid.* **96**, 106802 (2006); B. A. Bernevig, T. L. Hughes, and S. C. Zhang, *Science* **314**, 1757 (2006).
- <sup>26</sup>See, e.g., *The Quantum Hall Effect*, edited by R. E. Prange and S. M. Girvin (Springer, New York, 1987), and references therein.
- <sup>27</sup>D. J. Thouless, M. Kohmoto, M. P. Nightingale, and M. den Nijs, *Phys. Rev. Lett.* **49**, 405 (1982); M. Kohmoto, *Ann. Phys.* **160**, 343 (1985).
- <sup>28</sup>L. Fu and C. L. Kane, *Phys. Rev. B* **74**, 195312 (2006); **76**, 045302 (2007).
- <sup>29</sup>A. P. Schnyder, S. Ryu, A. Furusaki, and A. W. W. Ludwig, *Phys. Rev. B* **78**, 195125 (2008).
- <sup>30</sup>X. L. Qi, T. L. Hughes, S. Raghu, and S. C. Zhang, *Phys. Rev. Lett.* **102**, 187001 (2009); R. Roy, e-print arXiv:cond-mat/0608064; e-print arXiv:0803.2881; M. Sato, *Phys. Rev. B* **79**, 214526 (2009); **81**, 220504(R) (2010).
- <sup>31</sup>A. P. Schnyder, P. M. R. Brydon, D. Manske, and C. Timm, *Phys. Rev. B* **82**, 184508 (2010); S. Ryu, A. P. Schnyder, A. Furusaki, and A. Ludwig, *New J. Phys.* **12**, 065010 (2010).
- <sup>32</sup>L. Fu and C. L. Kane, *Phys. Rev. Lett.* **100**, 096407 (2008); **102**, 216403 (2009); J. Nilsson, A. R. Akhmerov, and C. W. J. Beenakker, *ibid.* **101**, 120403 (2008); A. R. Akhmerov, J. Nilsson, and C. W. J. Beenakker, *Phys. Rev. Lett.* **102**, 216404 (2009); M. Sato, Y. Takahashi, and S. Fujimoto, *ibid.* **103**, 020401 (2009); *Phys. Rev. B* **82**, 134521 (2010); Y. Tanaka, T. Yokoyama, and N. Nagaosa, *Phys. Rev. Lett.* **103**, 107002 (2009); K. T. Law, P. A. Lee, and T. K. Ng, *ibid.* **103**, 237001 (2009).
- <sup>33</sup>J. Linder, Y. Tanaka, T. Yokoyama, A. Sudbo, and N. Nagaosa, *Phys. Rev. Lett.* **104**, 067001 (2010); *Phys. Rev. B* **81**, 184525 (2010); M. Sato and S. Fujimoto, *Phys. Rev. Lett.* **105**, 217001 (2010).
- <sup>34</sup>J. Alicea, *Phys. Rev. B* **81**, 125318 (2010); J. D. Sau, R. M. Lutchyn, S. Tewari, and S. Das Sarma, *Phys. Rev. Lett.* **104**, 040502 (2010); Y. Asano, Y. Tanaka, and N. Nagaosa, *ibid.* **105**, 056402 (2010); V. Shivamoggi, G. Refael, and J. E. Moore, *Phys. Rev. B* **82**, 041405(R) (2010); K. Flensberg, *ibid.* **82**, 180516(R) (2010); R. Shindou, A. Furusaki, and N. Nagaosa, *ibid.* **82**, 180505 (2010); L. Mao and C. Zhang, *ibid.* **82**, 174506 (2010); T. Neupert, S. Onoda, and A. Furusaki, *Phys. Rev. Lett.* **105**, 206404 (2010).
- <sup>35</sup>When the symmetry of the singlet component of pair potential is  $d_{xy}$ -wave ( $d_{x^2-y^2}$ -wave), the number of the sign change of the real or imaginary part of triplet one on the Fermi surface is two (six). Thus, we call the mixed pair potential the  $d_{xy} + p$ -wave ( $d_{x^2-y^2} + f$ -wave).
- <sup>36</sup>M. Matsumoto and H. Shiba, *J. Phys. Soc. Jpn.* **64**, 1703 (1995).
- <sup>37</sup>M. Sato *et al.*, in preparation.
- <sup>38</sup>S. Kashiwaya, Y. Tanaka, N. Yoshida, and M. R. Beasley, *Phys. Rev. B* **60**, 3572 (1999).
- <sup>39</sup>A. P. Schnyder, S. Ryu, e-print arXiv:1011.1438.